

1 **Active, long-lived upper-plate splay faulting revealed by thermochronology in the Alaska**
2 **subduction zone**

3 Suoya Fan¹, Kristin D. Morell¹, Donald M. Fisher², Hugues Raimbourg³, Vincent Famin^{4,5},
4 Kristijan Rajič⁶

5 1. Department of Earth Science, University of California, Santa Barbara, Santa Barbara, CA,
6 USA

7 2. Department of Geosciences, Pennsylvania State University, University Park, PA, USA.

8 3. Institut des Sciences de la Terre d'Orléans, Université d'Orléans/CNRS/BRGM UMR7327,
9 1A Rue de la Ferrollerie, Orléans 45100, France

10 4. Université Paris Cité, Institut de Physique du Globe de Paris, Paris, France

11 5. Laboratoire Géosciences Réunion, Université de La Réunion, Saint-Denis, France

12 6. Department of Earth Sciences, Durham University, Science Laboratories, South Road,
13 Durham DH1 3LE, UK

14

15 **Keywords:**

16 Splay Fault; Forearc Tectonics; Alaska Subduction Zone; Thermochronology; Exhumation
17 History

18 **Highlights:**

- 19 ● Exhumation history revealed by thermochronology in the Alaska forearc region
20 ● Persistent inboard deformation along a highly active forearc splay fault since 6-7 Ma
21 ● Long-term slip rate and deep geometry estimations of the Kodiak Shelf Fault
22 ● Upper-plate architecture may control splay fault development and long-term activity

23

24 **Abstract**

25 The lack of subaerial forearc geological records in active subduction zones has hindered
26 our understanding of the roles of upper-plate structures and their interactions with plate interface
27 processes in accommodating forearc deformation. Forearc splay faults, a type of upper-plate
28 structure, are of particular interest due to their high efficiency in triggering tsunamis during great
29 earthquakes. The coastal area of the Kodiak Islands, Alaska, USA exhibits stratigraphic and
30 geomorphologic records of Miocene to Recent vertical tectonism and Quaternary thrust faults,
31 suggesting potential splay-fault-involved deformation over geological timescales. To better
32 understand the mechanisms of forearc long-term strain accumulation and the roles of splay
33 faults, we investigate the spatial and temporal pattern of recent forearc exhumation in the Kodiak
34 accretionary prism by conducting zircon and apatite (U-Th)/He (ZHe and AHe)
35 thermochronologic analyses and thermal history modeling. These results are supplemented by
36 field investigations, detrital zircon geochronology analyses and offshore active fault mapping.
37 Most of the ZHe ages record cooling through the ZHe closure temperature in the late Eocene-
38 early Oligocene, temporally and spatially consistent with the Eocene-early Oligocene broad
39 antiformal exhumation previously documented by zircon and apatite fission track
40 thermochronological ages. However, the AHe ages record cooling through the AHe closure
41 temperature from early Miocene to Pliocene and exhibit an overall trenchward younging trend,
42 with all the Pliocene ages (3-5 Ma) in the regions closest to the trench. Our thermal history
43 modeling and field survey suggest that the trenchward coastal area of the Kodiak Islands
44 experienced a change from early-middle Miocene basin subsidence to recent deformation and
45 rapid uplift from 6-7 Ma to recent, while the rest of the island experienced an early-middle
46 Miocene decrease in the prolonged exhumation from the Eocene-Oligocene. The newly revealed

47 long-term exhumation pattern resembles the estimated uplift patterns based on elevated marine
48 terraces and geodetic data. The early-middle Miocene change in exhumation pattern might be
49 caused by a change in the dominant deformation mechanism affecting the Kodiak Islands, from
50 broad underplating along the subduction interface mainly during the Eocene-Oligocene to
51 hanging-wall uplift due to an active crustal splay thrust fault system since the late Miocene (the
52 Kodiak Shelf Fault). We further discuss the dip-slip rate and geometry of the Kodiak Shelf Fault
53 system and how inherited forearc upper-plate structures and lithology may affect forearc fluid
54 distribution and facilitate the development and persistent deformation of the Kodiak Shelf Fault
55 system.

56 **1. Introduction**

57 Investigating the long-term activity, geometry, lifespan, and evolution of forearc upper-
58 plate structures in subduction zones is critical to understanding the growth mechanisms of
59 accretionary complexes, which involve complex and dynamic interactions between plate-
60 interface and upper-plate processes. Many studies have aimed to better understand these
61 interactions by correlating upper-plate structures, topography, and basins with subduction
62 interface properties and earthquake patterns (e.g., Wells et al., 2003; Saillard et al., 2017;
63 Dielforder et al., 2020; Jolivet et al., 2020; Michel-Wolf et al., 2022; Oryan et al., 2024). Deep-
64 rooted crustal splay faulting, for example, can be a major thickening mechanism in the forearc,
65 as indicated by out-of-sequence thrusts archived in exposed forearc accretionary complexes, such
66 as the Kodiak accretionary complex in Alaska, USA (Rowe et al., 2009; Farris, 2010; Wilson,
67 2013). The active equivalents of these faults, forearc active splay faults, tend to be located near
68 the rheological transition at the up-dip edge of the seismogenic zones (Wang and Hu, 2006;
69 Kimura et al., 2007; Wang and Morgan, 2022). This observation and records of their direct

70 involvement in tsunami-triggering processes during great earthquakes, further highlights the
71 significance of understanding active splay faults in assessing seismic and tsunami hazards (e.g.,
72 Plafker, 1965; Cummins and Kaneda, 2000; Sibuet et al., 2007). However, the long-term history,
73 including the initiation, lifespan, cessation, and reactivation of currently active splay faults, is
74 rarely well studied.

75 Splay faults have been proposed to efficiently transfer deep displacement to the surface,
76 fostering tsunami genesis (Moore et al., 2007; Wendt et al., 2009; van Zelst et al., 2022).

77 Previous studies suggest that the coseismic rupture of a forearc splay fault in the Prince William
78 Sound fostered the genesis of a large tsunami in the Alaska subduction zone during the 1964
79 M9.2 Great Alaska earthquake (Plafker, 1965; Suito and Freymueller, 2009; Suleimani and
80 Freymueller, 2020) and its repeated ruptures have contributed to long-term permanent forearc
81 uplift (Liberty et al., 2013; Haeussler et al., 2015; DePaolis et al., 2024). The involvement of
82 splay fault rupture has also been suggested in other great tsunamigenic subduction zone
83 earthquakes, such as the 1944 M8.1 Tonankai earthquake and the 1946 M8.3 Nankai earthquake
84 in Japan (Cummins and Kaneda, 2000; Park et al., 2002), as well as the 2004 Mw9.2 Sumatra
85 earthquake (Sibuet et al., 2007).

86 Splay faults located in the general region near the up-dip edge of the seismogenic zone
87 have been well-documented, with examples such as Nankai (Park et al., 2002; Kimura et al.,
88 2007; Moore et al., 2007; Strasser et al., 2009), Sumatra (Cook et al., 2014; Qin et al., 2024), and
89 Hikurangi (Barker et al., 2018; Barnes et al., 2020). Similarly, offshore surveys in the Alaska
90 subduction zone have primarily focused on the forearc frontal part straddling the up-dip limit of
91 the seismogenic zone (e.g., Li et al., 2018; von Huene et al., 2021). However, the geometry and
92 long-term evolution of active splay faults located in the forearc farther inboard are generally

93 poorly understood, in large part because direct geological studies of these structures are often
94 hindered by a lack of subaerial exposures and require deep seismic data.

95 The Kodiak Islands in the forearc of the highly-coupled Alaska subduction zone, located
96 ~140 km from the trench, is an ideal area to probe the geometry and rates of splay faulting in the
97 inner forearc. The trenchward coastal area of the Kodiak Islands is located approximately above
98 the present down-dip edge of the seismogenic zone and exhibits stratigraphic and
99 geomorphologic records of Miocene to Recent vertical tectonism and includes a series of
100 Quaternary active faults (e.g., Clendenen et al., 1992; Carver et al., 2008; Elliott and
101 Freymueller, 2020). These active faults are interpreted as a part of the Kodiak Shelf Fault Zone,
102 a major offshore crustal splay fault zone that has been proposed to have ruptured during the 1964
103 Great Alaska earthquake and was the potential source of a local Kodiak Islands tsunami (Ramos
104 et al., 2022). These co-located indicators of forearc deformation across a wide range of
105 timescales suggest a potential causal relationship between the persistent activity of the Kodiak
106 Shelf Fault Zone and long-term upper-plate vertical tectonism, as evidenced by uplifted and
107 deformed Miocene shelf-basin strata. However, testing this hypothesis requires a better
108 understanding of the Kodiak Shelf Fault Zone, including its kinematics, deep geometry,
109 deformation rates, and slip history.

110 To better understand the rates, history, and spatial distribution of forearc deformation
111 across the Kodiak Shelf Fault Zone, its relation to deep accretionary complex structures and its
112 connectivity with the subduction interface, we investigate the spatial-temporal exhumation
113 patterns of the Kodiak Islands with a focus on the post-Oligocene history of the trenchward
114 coastal area. We conduct new low-temperature zircon and apatite (U-Th)/He (ZHe and AHe)
115 thermochronology analyses together with thermal history modeling and detrital zircon

116 geochronologic analyses. The AHe ages reveal a previously unrecognized rapid exhumation
117 pattern that we interpret to be primarily controlled by displacement along the Kodiak Shelf Fault
118 Zone. The ZHe and AHe ages suggest a significant change in forearc dominant deformation style
119 in the early-middle Miocene. The new deformation pattern after the style change indicates
120 persistent deformation of the Kodiak Shelf Fault Zone from 6-7 Ma to present. We further infer a
121 deep fault geometry and compare it with published forearc geophysical data to discuss how the
122 inherited upper-plate structures and lithologic architecture may affect regional fluid distribution
123 and facilitate the development and persistent deformation of the Kodiak Shelf Fault.

124 **2. Geology**

125 **2.1. Tectonostratigraphy of the Kodiak Islands**

126 The Kodiak Islands represent the subaerial part of the Kodiak accretionary complex,
127 comprising a series of trench-parallel-striking rock packages that decrease in age and
128 metamorphic grade trenchward (Moore et al., 1983) (Fig. 1). These rock packages were accreted
129 episodically since the Jurassic through underplating or frontal accretion (Moore and Allwardt,
130 1980; Byrne and Fisher, 1987; Fisher and Byrne, 1987; Fisher and Byrne, 1992; Clendenen et al.,
131 2003; Rajič et al., 2023). The northwestern edge of the Kodiak Islands comprises an island arc
132 assemblage of late Triassic to early Jurassic ages and the Jurassic Raspberry Schist (Carden et
133 al., 1977; Burns, 1985; Roeske et al., 1989). The Border Ranges Fault juxtaposes these rocks
134 against the Uyak Complex, a tectonic *mélange* with rocks that contain fossils of mid-Permian to
135 mid-early Cretaceous age (Connelly, 1978). The Uyak Complex is in tectonic contact with the
136 Kodiak Formation southeast of it along the Uganik Thrust (Moore, 1978; Rowe et al., 2009).

137 The Kodiak Formation is a mostly structurally coherent, thick sequence of deep-water
138 turbidites, including interbedded slates, siltstones, and sandstones, deposited in the Maastrichtian

139 ~70 Ma ago (Byrne and Fisher, 1987; Sample and Reid, 2003). It occupies most of the Kodiak
140 Islands and forms a regional anticlinorium (Sample and Moore, 1987; Fisher and Byrne, 1992;
141 Rajič et al., 2023). The Kodiak Formation is separated from the Paleocene Ghost Rocks
142 Formation by the Contact Fault (Fig. 1; Farris, 2010; Wilson, 2013). The Ghost Rocks Formation
143 consists of a structurally coherent unit in the northwest and a tectonic *mélange* in the southeast
144 (Byrne, 1984). The accretion of the Kodiak Formation and Ghost Rocks Formation occurred
145 from the late Cretaceous to the early Paleogene (Byrne, 1984; Byrne and Fisher, 1987), and the
146 youngest temporal limit is well bracketed by the ages of temporally close (about 58-62 Ma) but
147 widely distributed intrusive rocks (Moore et al., 1983; Byrne and Fisher, 1987; Sample and
148 Moore, 1987; Farris et al., 2006; Farris, 2010). These intrusive rocks are mostly andesite and
149 granodiorite with some mafic rocks and are interpreted to be caused by west-to-east migrating
150 ridge subduction and the interaction of MORB-type magmas with the metasedimentary rocks in
151 the accretionary prism (Moore et al., 1983; Haeussler et al., 2003; Farris et al., 2006). The largest
152 pluton is the Kodiak Batholith, the exposure of which trends sub-parallel with the long axis of
153 the islands (Fig. 1).

154 The Eocene Sitkalidak Formation, in fault contact with the Ghost Rocks Formation, is a
155 deep-sea fan sequence consisting of sandstone, siltstone, mudstone, and conglomerate and
156 outcrops along the southeastern edge of the Kodiak Islands (Figs. 1 and 2), including the Ugak
157 Island (Nilsen and Moore, 1979; Moore and Allwardt, 1980). It contains two structural units: a
158 less deformed portion interpreted as a shortened slope basin or slope apron deposit and a strongly
159 deformed portion featured by landward verging folds and thrusts interpreted as trench-filling
160 sediment offscraped from the lower plate (Moore and Allwardt, 1980).

161 Oligocene-Pleistocene slope basin fill overlies the Ghost Rocks and Sitkalidak
162 Formations above an angular unconformity, and it contains several units of different ages along
163 the southeastern margin of the Kodiak Islands (Moore and Allwardt, 1980; Clendenen et al.,
164 1992; Marincovich and Moriya, 1992). In the Narrow Cape area, the sequence above the
165 unconformity is the slightly younger middle Miocene Narrow Cape Formation comprising
166 shallow marine sandstone and sandy siltstone, with interbedded conglomerate beds (Moore et al.,
167 1983). The age of the Narrow Cape Formation is interpreted to be 15-16 Ma based on well-dated
168 faunas (Marincovich and Moriya, 1992). The Oligocene-Miocene unconformity has been
169 interpreted to be correlated seaward to an unconformity visible in seismic reflection profiles in
170 the offshore region (Fisher and Holmes, 1980; Moore and Allwardt, 1980; Clendenen et al.,
171 1992). The offshore part of the post-unconformity basin has continuously received sediments up
172 until the present day. The current trenchward boundary of the shelf-basin is approximately
173 located at the present-day shelf break, about 60-80 km trenchward from the landward boundary
174 exposed on the Kodiak Islands. The subaerial basin recorded by the Narrow Cape Formation in
175 the Kodiak coastal area may represent the deformed and uplifted part of this same basin.

176 **2.2. Cretaceous-Cenozoic Deformation, Exhumation and Active Tectonics**

177 **2.2.1 Cretaceous to Miocene**

178 Two main episodes of deformation and exhumation before the Miocene have been
179 recognized in the Kodiak Islands. The first episode is represented by the accretion of the Kodiak
180 and Ghost Rocks Formations, mainly through underplating along the subduction interface from
181 the late Cretaceous to the early Paleocene. Evidence for underplating includes the regional
182 anticlinorium, duplex structures in both mesoscopic and map scales, and across-strike changes in
183 deformation style, magnitude and structural orientation (Sample and Fisher, 1986; Fisher and

184 Byrne, 1987; Sample and Moore, 1987; Fisher and Byrne, 1992; Rajič et al., 2023). The peak
185 temperature and amount of exhumation experienced by the Kodiak and Ghost Rocks Formations
186 also mimic the antiformal pattern with the highest magnitude in the core of the anticlinorium
187 (Clendenen et al., 2003; Rajič et al., 2023). The second episode of exhumation and thickening
188 occurred from Eocene to Oligocene and has been interpreted as a result of trenchward-
189 propagating underplating. Evidence for this process is based on a thermochronologic study
190 involving zircon and apatite fission track (ZFT and AFT) dating that shows cooling ages become
191 younger trenchward from the northwestern limit of the Kodiak Formation to the Kodiak
192 Batholith (Clendenen et al., 2003). Moreover, an offshore seismic reflection profile northeast of
193 the Kodiak Islands exhibits arched reflectors that coincide with a thick low-velocity zone below
194 the Mesozoic and Paleocene accretionary prism, consistent with underplating (Byrne, 1986;
195 Moore et al., 1991; Ye et al., 1997).

196 **2.2.2 Miocene to Quaternary**

197 Paleoseismic, geodetic, stratigraphic, and field data together provide several lines of
198 evidence for Quaternary-active deformation within the Narrow Cape and surrounding area of the
199 Kodiak Islands. Geomorphology and paleoseismology surveys in the Narrow Cape area have
200 identified several near-vertical faults that have been reported to accommodate both vertical and
201 strike-slip Quaternary displacement (Carver et al., 2008). Carver et al. (2008) documented fault
202 activity spanning the latest Pleistocene and Holocene and suggested the faults offset a marine
203 terrace by up to 20 m and offset channels left-laterally by up to 30-35 m. Carver et al. (2008)
204 interpreted the major faults as part of the Kodiak Shelf Fault Zone, a ~200-km-long margin-
205 parallel active splay fault system (Fig. 1). In the field, we observed these faults cross-cutting the
206 sub-horizontal angular unconformity separating the Ghost Rocks and Narrow Cape Formations

207 by as much as ~30 m in the modern sea cliff (Fig. 2). The angular unconformity and the Narrow
208 Cape Formation above it have been gently folded into an anticline and syncline; these folds are
209 likely related to these active structures. Carver et al. (2008) recognized a group of coastal
210 surfaces, characterized by a locally uniform elevation, planar sub-horizontal abrasion surfaces,
211 with a sharp back-edge that parallels the shoreline. They interpreted them as raised wave-cut
212 marine terraces formed during Marine Isotope Stage (MIS) 5e (120-130 ka). The elevation of
213 these marine terraces across the Kodiak Islands also increases abruptly in the Narrow Cape area,
214 suggesting a 3-5 times higher Quaternary uplift rate of the Narrow Cape area than areas arcward
215 (Carver et al., 2008), although the source of this reported uplift is not described in previous
216 literature. Campaign GNSS data collected over an 8-year period also exhibit the highest across-
217 strike velocity spatial gradient in this region, suggesting left-lateral transpressional strain, in the
218 Narrow Cape area (Sauber et al., 2006; Carver et al., 2008). The area also lies roughly above the
219 locked-creeping transition zone along the subduction interface (Elliott and Freymueller, 2020).

220 In the trenchward region offshore within 15 km of the Narrow Cape area of the Kodiak
221 Islands, the Kodiak Shelf Fault Zone has been recognized and mapped based on seismic
222 reflection images and bathymetry data (Ramos et al., 2022). The fault system contains multiple
223 strands offshore, among which the most recognizable is the Ugak Thrust, located ~5 km seaward
224 of Ugak Island (Figs. 1 and 3). Based on seismic reflection profiles, these faults have been
225 reported to be landward dipping at 65-80° close to the seafloor and may merge at depth (Ramos
226 et al., 2022). The Ugak Fault offsets the seafloor, forming a prominent bathymetric scarp, as
227 much as 30 m high, and extends at least 80 km in length. Other high-angle faults have been
228 previously identified cutting the slope basin strata but their recent activity remains unclear
229 (Fisher and Holmes, 1980). Northeast of the Kodiak Islands, in the Prince William Sound

230 segment, a similar splay fault system in the equivalent structural location in the forearc has been
231 recognized and thought to have ruptured during the 1964 M9.2 earthquake, but there is no direct
232 evidence connecting it to the Kodiak Shelf Fault Zone (Liberty et al., 2013; Haeussler et al.,
233 2015; Liberty et al., 2019; DePaolis et al., 2024). Although these previous studies provide
234 evidence for Quaternary activity, mainly in the form of faulting and folding in the Narrow Cape
235 region, how long these structures have been active, their exhumation histories, throw rates, and
236 potential relationship to the underplating and duplexing structures remain poorly understood.

237 **3. Thermochronology and Geochronology**

238 **3.1. Methods and samples**

239 To investigate post-Oligocene to Quaternary exhumation mechanisms of the Kodiak
240 Islands, we conducted ZHe and AHe thermochronologic analyses on samples collected along a
241 trench-perpendicular transect (Fig. 1; Tables 1). The closure temperatures of the zircon and
242 apatite thermochronometers are affected by various factors, such as the chemical composition of
243 the minerals, concentration of radiation damage, grain size and cooling rate (Reiners et al., 2004;
244 Reiners, 2005) but typically range from ~ 170-190 °C (Reiners et al., 2004) and ~ 45-70 °C
245 (Flowers et al., 2009). We obtained 19 ZHe and 13 AHe ages from 19 samples across the Kodiak
246 Islands (Fig. 1 and 2; Tables 1 and S1), from the Uyak Complex along the landward coast to
247 Ugak Island in the trenchward coastal area. We increased sampling density in the southeastern
248 half of the transect. Our sampling strategy was to first attempt to sample 60-Ma plutonic rocks,
249 because we found that these samples contained the largest suitable apatite and zircon grains for
250 dating. When these rock types were not available along the transect, we also sampled low-grade
251 metamorphic rocks of the Kodiak and Ghost Rocks Formation, sandstones from the Sitkalidak
252 and Narrow Cape Formations, and two samples from the Uyak Complex. We collected samples

253 with the largest visible grain size. The supplementary information contains the details of our
254 sample processing and dating analysis.

255 In addition to thermochronology, we also conducted detrital zircon (U-Pb)
256 geochronologic analyses on two Narrow Cape samples and one Sitkalidak Formation sample to
257 understand their provenance and depositional ages. The Sitkalidak Formation sample was
258 collected from Ugak Island, and the Narrow Cape Formation samples are collected directly
259 above its unconformable contact with the Ghost Rocks Formation (Fig. 2).

260 **3.2. Results**

261 The AHe ages range from 20 to 3 Ma, showing an overall decrease in age trenchward for
262 the 30-km-long area northeast of Ugak Island (Figs. 2 and 4). The ages in the region from the
263 Uyak Complex to the Contact Fault are generally spatially invariant at 15-20 Ma for 70 km
264 across strike. Neither the Uganik thrust nor the Contact Fault show variations in cooling ages
265 across them, suggesting no significant faulting-related exhumation along these onshore major
266 faults since the Miocene. The AHe cooling ages from the plutonic rock that intruded into the
267 Ghost Rocks Formation and further trenchward are all younger than 10 Ma, and the four samples
268 closest to the offshore Kodiak Shelf Fault Zone, within 20 km from the Ugak Fault, yielded
269 Pliocene cooling ages (3-5 Ma). Two of the Pliocene cooling ages are derived from the youngest
270 grain age in each sample from the Narrow Cape Formation. These samples exhibit a wide
271 dispersion of AHe grain ages, including ages younger than the middle Miocene depositional age,
272 indicating partial thermal resetting of the samples during burial heating. Because their youngest
273 grain ages (4.1 ± 0.2 Ma and 5.1 ± 0.2 Ma) are close to the mean aliquot ages of the fully
274 thermally-reset Sitkalidak Formation (3.3 ± 0.3 Ma) and Ghost Rocks Formation (4.3 ± 0.6 Ma),

275 we interpret these youngest grains as being fully or nearly fully reset before recent cooling
276 through the AHe partial retention temperature zone.

277 The ZHe age range overall overlaps with the published AFT ages and is younger than the
278 ZFT ages in the area of data coverage (>38 km on the age-distance profile in Fig. 4). These ZHe
279 ages exhibit an overall decrease in cooling ages from 52-54 Ma for samples of the early
280 Cretaceous Uyak Complex on the landward side of the Kodiak Islands to 30-34 Ma of the
281 Kodiak Batholith (58-59 Ma U-Pb zircon ages; Farris, 2010). This age spatial variation pattern
282 resembles the AFT age spatial pattern reported by Clendenen et al. (2003).

283 The ZHe, AFT and ZFT samples all progressively decrease in age from the arcward coast
284 to the Kodiak Batholith. In contrast, the ZHe ages further trenchward, located about 0-38 km on
285 the age profile (Fig. 4), are invariant in age along strike, with samples in this region close to or
286 slightly older than the ZHe ages of the Kodiak Batholith. Among them, the five samples closest
287 to the Uyak Thrust are not thermally reset after deposition: four samples from the Narrow Cape
288 Formation and Sitkalidak Formation yield dispersed grain ages older than their depositional ages.
289 One sample from the Ghost Rocks formation in the Narrow Cape area close to the unconformity
290 generated grain ages of 60-67 Ma, much older than the ZHe ages of two other Ghost Rocks
291 Formation samples (30 and 35 Ma) near a basalt intrusion and the ages of the pluton rock
292 intruded into the Ghost Rocks Formation.

293 The U-Pb detrital zircon ages of the Sitkalidak Formation and the Narrow Cape
294 Formation samples mostly range from 50 Ma to 220 Ma (Table S2). The probability density
295 curve peaks at around 60 Ma, a broad high age spectrum ranging from 60 to 110 Ma, and a low
296 broad age spectrum of 130-220 Ma, mainly straddling the Jurassic (Fig. 5). The youngest ages
297 are much older than the depositional ages of the two formations (Eocene-early Oligocene and

298 mid-late Miocene, respectively); therefore, they do not provide meaningful estimation of
299 maximum depositional ages. The 60 Ma peak coincides with the narrow age range of the widely
300 distributed igneous rocks, represented by the Kodiak Batholith. The broad high spectrum of the
301 Cretaceous ages and the low, broad spectrum of the Jurassic ages can be correlated with the
302 widely distributed Cretaceous Kodiak Formation and the Jurassic accretionary complex and
303 plutons on the northwestern edge of the Kodiak Islands. Therefore, the data support the idea that
304 the Sitkalidak and Narrow Cape Formations might be mainly sourced from the Kodiak Islands
305 and record the broad exhumation of the island during their deposition from the Eocene to
306 Miocene.

307 **4. Thermal History Modeling**

308 The variations in thermochronology ages along the transect and the source-to-sink history
309 associated with the deposition of the Sitkalidak and Narrow Cape Formations, all indicate spatial
310 variations in erosion and deposition of the Kodiak Islands. To further investigate the magnitude
311 and timing of exhumation across the transect, we conducted one-dimensional thermal history
312 modeling using the HeFTy (Ketcham, 2005) program with our new data. The temperature-time
313 constraints used in the HeFTy modeling were based on geological context, published nearby
314 thermochronologic data from Clendenen et al. (2003) and peak temperature estimations from
315 Rajič et al. (2023) (Figs. 2 and 6). Considering the higher data density and higher cooling age
316 contrast in the southeastern half of the Kodiak Islands, we selected five modeling localities
317 between the Kodiak Batholith, where the minimum ZHe, AFT, and ZFT ages have been
318 reported, and the Ghost Rocks Formation in the trenchward coastal area of the islands, where the
319 youngest AHe ages are located (Fig. 4). Models 1 and 2 are the farthest and of similar distance
320 from the trench, but they are 43 km apart along strike. Models 2 to 5 are progressively closer to

321 the trench. For detailed descriptions, modeled age data, thermal history constraints, and the
322 geological context considered in each model, refer to the text and Table S3 in the Supplementary
323 Information.

324 The thermochronologic data and modeling results show that the previously recognized
325 Eocene-Oligocene broad cooling lasted until the early Miocene (15-20 Ma). After that, the
326 trenchward coastal area and the central part of the Kodiak Islands exhibit distinct thermal
327 histories. During approximately the middle-late Miocene, the central part of the Kodiak Islands
328 (Models 1-3) changed to a slow cooling path, while the trenchward coastal area (Models 4 and
329 5), mainly the area of Ghost Rocks Formation and Narrow Cape Formation, experienced a
330 transition from cooling to reheating, which was associated with the change from erosion to
331 deposition along the angular unconformity beneath the forearc basin sediments of the Narrow
332 Cape Formation. Some possible temperature-time paths with a good fit suggest a possible short
333 period of accelerated cooling during the transitional phase (around 15-20 Ma) preceding the slow
334 cooling phase in the central part of Kodiak Islands; but this possible acceleration in cooling is not
335 required in all temperature-time paths with a good fit. Since the latest Miocene, the trenchward
336 coastal area of the islands has been experiencing rapid cooling.

337 **5. Discussion**

338 **5.1. Exhumation History**

339 Our new ZHe ages and published ZFT and AFT ages are consistent with the previous
340 interpretation that the Kodiak Islands experienced broad antiformal thickening and exhumation
341 from the Eocene to Oligocene that straddles the Kodiak Islands (Clendenen et al., 2003).
342 Structural and geophysical observations suggest the underplating process might have caused this
343 regional thickening and exhumation pattern with a hinge line located in the central part of the

344 Kodiak Islands (e.g., Byrne, 1986; Fisher and Byrne, 1992; Ye et al., 1997). Our ZHe ages and
345 fission track ages of previous researchers (Clendenen et al., 2003) agree with this pattern as
346 evidenced by their across-strike long-wavelength gradual change with the youngest ages in the
347 Kodiak Batholith area in the central part of the Kodiak Islands (Fig. 4). This interpretation is
348 further supported by Raman spectroscopy of carbonaceous materials that reveals a similar pattern
349 of peak temperature: relatively high-temperature records broadly distributed in the central part of
350 the Kodiak Islands with decreased temperature records in both trenchward and landward coastal
351 areas (Rajič et al., 2023).

352 Our new AHe ages reveal a previously unrecognized cooling age pattern along the
353 transect (Fig. 4). In the northwest, the AHe ages are relatively invariant, ranging from 15-20 Ma
354 for ~60 km across strike from the Uyak Complex to the Kodiak Batholith. Moving trenchward,
355 in the area occupied by the Ghost Rocks *mélange* and Narrow Cape Formations, the ages
356 decrease to 4-5 Ma. Finally, at Ugak Island, ~5 km from the Ugak Fault, the AHe ages further
357 decrease to 3 Ma. This AHe age pattern suggests that the previously recognized Eocene-
358 Oligocene broad exhumation might have extended into the early Miocene in the central part of
359 the Kodiak Islands, but the late Miocene-Pliocene exhumation may have been affected by a
360 different deformation mechanism than the antiformal deformation that was occurring during the
361 Eocene to Oligocene.

362 The difference in uplift and subsidence history between the trenchward coastal area of the
363 Kodiak Islands and the area farther arcward is investigated with our one-dimensional thermal
364 history models that incorporate constraints from geological observations (Fig. 6). In the area
365 landward of the Contact Fault, represented by Models 1-3, the prolonged cooling in the
366 Paleogene lasts through the Miocene. However, the cooling rate decreased after the early-middle

367 Miocene (20-15 Ma) and has since maintained a slow cooling rate. In the meantime, the
368 trenchward coastal area of the Kodiak Islands, the area represented by Models 4 and 5,
369 experienced a more complicated thermal history involving two cooling phases interrupted by a
370 reheating process.

371 The first cooling episode of the trenchward coastal area of the Kodiak Islands might be
372 caused by exhumation associated with the prolonged Oligocene to Miocene broad antiformal
373 folding event, which may be related to underplating (Fig. 4). The unconformity between the
374 Ghost Rocks and the Narrow Cape Formations, indicating uplift and erosion prior to the middle
375 Miocene, may have formed during this period. The reheating process in Models 4 and 5
376 corresponds to the deposition of the Narrow Cape Formation, a subsidence and burial event, and
377 temporally overlaps with the transition from fast to slow cooling in Models 1-3 (Fig. 6). These
378 models suggest that the shelf subsidence in the Narrow Cape area indicated by the Narrow Cape
379 basin formation is synchronous with a decrease, if not cessation, of the underplating process
380 northwest of the basin below the Kodiak Islands. Previous stratigraphic and lithologic data of the
381 shelf basin (Clendenen et al., 1992), our new detrital zircon U-Pb age spectrum, and the overlap
382 between the range of the detrital ZHe ages of the Narrow Cape Formation and the cooling age
383 range landward of the shelf basin, all suggest that the Kodiak Islands is the main source of
384 sediment in the shelf basin along the Kodiak Islands coast in this period.

385 The second rapid cooling episode after the mid-late Miocene deposition and reheating
386 along the trenchward coast of the Kodiak Islands (Models 4 and 5) is missing in the area
387 represented by Models 1-3 (Fig. 6). Our thermal modeling results suggest that the initiation of
388 this exhumation episode is no later than ~6 Ma (Fig. 6). The youngest basin fill along the Kodiak
389 Islands coast, the late Pliocene-Pleistocene Tugidak Formation, locally overlies the along-strike

390 equivalent of the Narrow Cape Formation on the Trinity Island about 150 km southwest of our
391 study area (Clendenen et al., 1992), suggesting that the initiation time of the latest rapid coast
392 uplift should not be much older than the late Pliocene. The latest Miocene Albatross sedimentary
393 sequence, the shelf basin record on the Trinity Islands, records a transition from a shallow-
394 marine depositional environment to a terrestrial environment, suggesting an uplift process
395 (Clendenen et al., 1992). These observations bracket the initiation time of the rapid uplift and
396 exhumation at about 6-7 Ma.

397 **5.2. Miocene-Quaternary Exhumation Pattern and the Kodiak Shelf Fault Zone**

398 Assuming a thermal gradient of about 30 °C/km (Moore and Allwardt, 1980) and a peak
399 temperature of 120 °C (Rajič et al., 2023) results in an exhumation rate of ~0.6-0.7 mm/yr and a
400 total exhumation of about 4 km for the Miocene-Quaternary episode. This estimated exhumation
401 rate is close to the inferred uplift rate of about 0.75 mm/yr based on the elevation of the uplifted
402 coastal surface, assuming the surface formed during 130–120 ka (Carver et al., 2008).

403 To better evaluate the spatial variations in the new Miocene-Recent exhumation pattern
404 revealed by the AHe ages, we calculated the exhumation rate for each AHe sample assuming
405 steady, vertical rock uplift and unchanging topography (van der Beek and Schildgen, 2023). The
406 results represent the averaged exhumation rate since the samples cooled through their closure
407 temperatures. In three calculations, we assumed three initial geothermal gradients at 25 °C/km,
408 30 °C/km, and 35 °C/km, respectively. The result shows that the exhumation rate increases
409 rapidly trenchward from about 0.1 mm/yr in the Kodiak Batholith area to about 0.5-0.7 mm/yr
410 near Ugak Island (Fig. 7). The highest exhumation rates are located in the hanging wall of the
411 Ugak Fault.

412 We also evaluate Quaternary uplift rates across the Kodiak Islands from the elevations of
413 previously reported marine terraces, assuming they formed during MIS 5e, at about 125 ka
414 following Carver et al. (2008). Although the terrace is not directly dated, Carver et al. (2008)
415 speculate that the terrace must date to ~130-120 ka because paleosea level during MIS 5e
416 represents the last time that paleosea level was higher than current sea level, and therefore is the
417 last time that sea level occupied the position of the modern coastline. Although the marine
418 terrace heights are likely affected by isostatic rebound following regional late Pleistocene
419 deglaciation (Carver et al., 2008), and the assumed terrace uplift rates overall are higher than the
420 calculated exhumation rates based on the AHe ages by about 0.15-0.2 mm/yr, they share a
421 similar spatial pattern regardless of their age (Fig. 7). This pattern is also similar to the pattern
422 revealed by current geodetic data, which shows the largest spatial gradient in the trenchward
423 coastal area of the Kodiak Islands (Carver et al., 2008). The similarity of deformation patterns
424 over decadal time spans represented by geodetics, millennial time scale recorded by marine
425 terraces, and Myr time scale recorded by thermochronology suggests that the present
426 deformation mechanism has controlled a persistent uplift pattern over a range of time scales.

427 Our ZHe ages and thermal modeling results, along with previous studies on rock cooling
428 history, structures, peak temperatures, and seismic reflection profiles suggest that underplating
429 along the plate interface could be the main mechanism of forearc wedge thickening in the
430 Eocene-Oligocene (Byrne, 1986; Sample and Fisher, 1986; Moore et al., 1991; Fisher and Byrne,
431 1992; Ye et al., 1997; Clendenen et al., 2003; Rajič et al., 2023). Although we cannot preclude
432 the possibility of a new underplating system below the trenchward coastal area, the short
433 wavelength (~10 Myr cooling age difference and a doubling of exhumation rate across 10-15
434 km) of the across-strike changes in the AHe age and exhumation rate suggests that underplating

435 is unlikely the determining cause of the new exhumation pattern. The Pliocene AHe ages
436 spatially coincide with the documented active faults in the Narrow Cape area and are within
437 about 20 km from the fault traces of the offshore Kodiak Shelf Fault Zone (Fig. 4), suggesting
438 that this exhumation episode is mainly affected by the hanging-wall uplift of the active Kodiak
439 Shelf Fault Zone. Therefore, the initiation of the Kodiak Shelf Fault Zone is likely also 6-7 Ma.
440 This interpretation is consistent with the lithologic study of the latest Miocene-Pliocene
441 Albatross sedimentary sequence on the hanging-wall side of the fault zone, which suggests an
442 upward decrease in clasts from the uplifted shelf break (decrease in chert and total absence of
443 calcareous shale in the upper part) and an increase in clasts from the Kodiak Islands as well as
444 the shallowing of the depositional environment from shallow marine to terrestrial (Clendenen et
445 al., 1992). The initiation of the Kodiak Shelf Fault Zone might have uplifted the basin in its
446 hanging wall and interrupted the transport path of clasts from the shelf break.

447 Assuming that exhumation is related to throw on the Kodiak Shelf Fault Zone, our new
448 results on spatial variations in exhumation rate can place constraints on the deep geometry of the
449 fault zone. Most of the Kodiak Islands have been experiencing slow exhumation after 15 Ma,
450 and the rapid Pliocene exhumation is limited in the trenchward coastal area approximately
451 southeast of the Contact Fault, close to the main offshore Kodiak Shelf Fault Zone traces (Fig.
452 7). This pattern suggests that the landward-dipping Kodiak Shelf Fault Zone may become gently
453 dipping beneath the Kodiak Islands (Fig. 8). Assuming the varied exhumation is caused by pure
454 dip-slip along the Kodiak Shelf Fault Zone with a fault bend separating a steep frontal ramp from
455 a deeper gentle flat, we semi-quantitatively estimate the deep geometry. If we assume that the
456 exhumation is balanced by uplift and the uplift rates are the vertical components of fault-slip
457 rates, we can calculate the correspondent fault slip rate and dip of the gentle decollement for a

458 given dip of the frontal thrust ramp. We use the calculated exhumation rates of Ugak Island (0.59
459 mm/yr for an initial geothermal gradient 30 °C/km) and the Kodiak Batholith (0.1 mm/yr) as
460 uplift rates above the two fault domains. For a frontal dip of 30, 40, 50 and 60 degrees, we
461 estimate the corresponding dip-slip rates are 1.15 mm/yr, 0.90 mm/yr, 0.75 mm/yr and 0.67
462 mm/yr, respectively, and the corresponding dips of the fault flat beneath the Kodiak Islands are
463 roughly 5, 6, 7 and 8 degrees respectively (Fig. 7). Assuming the bisector of the fault bend
464 projects to the exhumation rate change at the surface, we can construct the general fault
465 geometry. These slip rate estimations do not include lateral strike-slip components, but this
466 simplification does not affect geometry estimations because we assume only dip slip contributes
467 to uplift. We find that even a steep 60-degree Kodiak Shelf Fault Zone frontal thrust cannot
468 directly connect to the subduction interface (Hayes et al., 2018) before it becomes flat and
469 subparallel to the interface at a depth of about 20 km. The more realistic 30-degree frontal thrust
470 requires the fault flattening at a depth of about 12 km. The flat section can be approximately
471 correlated to an abrupt change in the seismically-determined V_p/V_s ratio within the wedge (Fig.
472 8, Wang et al., 2024). Therefore, the fault may root into deep structures and may be associated
473 with mechanical property changes within the wedge rather than the subduction interface. The
474 Contact Fault, which likely played a similar role to the KSFZ as an older out-of-sequence thrust
475 fault, may have been offset by younger faults or the active KSFZ at depth. If its shallow part is
476 active, it may branch into the KSFZ flat. A 30-degree geometry of the frontal thrust of the KSFZ
477 also requires a fault slip rate of 1.15 mm/yr, which is about 2% of the present plate convergence
478 rate of 57 mm/yr (DeMets et al., 1990). If so, only a small portion of the plate convergence has
479 been accommodated by the Kodiak Shelf Fault Zone since its presumed initiation at 6-7 Ma.
480 Elliott and Freymueller (2020) estimated GPS-data-derived left-lateral and compressional

481 deformation rates of 2.2 ± 0.3 mm/yr and 3.5 ± 0.4 mm/yr, respectively, approximately across
482 the Kodiak Shelf Fault Zone. The much higher geodetic compressional rate than our estimated
483 long-term dip-slip rate may suggest only a portion of the interseismic geodetic strain translates to
484 permanent deformation as fault slip along the Kodiak Shelf Fault, assuming the compression
485 remained at a higher rate throughout the history of the Kodiak Shelf Fault.

486 At shallow depths, the displacement may be distributed along multiple fault strands.
487 Ramos et al. (2022) previously recognized the Ugak Fault, the primary offshore strand of the
488 Kodiak Shelf Fault Zone, from bathymetry data and legacy seismic profiles. Using recent
489 bathymetry data and archived seismic images collected in 1975, we mapped more active fault
490 strands in the Ugak Island area (Figs. 3 and S1). They exhibit linear fault and/or fold scarps on
491 the seafloor. On the seismic reflective images, they offset young deposits and occasionally show
492 growth strata. Seismic images also show the Ugak Fault has the most prominent offset (Fig. S1).
493 Previous onshore geomorphologic and paleoseismological studies (e.g., Carver et al., 2008) and
494 our bedrock-structure survey along the coastal cliff in the Narrow Cape area also highlight
495 multiple high-angle faults. The high-angle faults we observed are in the core of a broad 3-km
496 wide anticline formed within the Narrow Cape Formation and its underlying unconformity. We
497 interpret them as shallow faults accommodating passive deformation above a blind thrust fault
498 strand below the broad anticline or as fault strands that mainly accommodate strike-slip
499 displacement and may merge together at depth (Fig. 8).

500 **5.3. Kodiak Shelf Fault Zone Development Mechanism**

501 Reactivation of inherited structures as a mechanism for upper-plate out-of-sequence
502 thrusting is common in many accretionary complexes, such as the Shimanto accretionary
503 complex in Japan (Fisher et al., 2019). The development of the Kodiak Shelf Fault Zone may

504 have exploited the preexisting upper-plate lithologic architecture. The fault system has developed
505 along an approximate boundary in the forearc between lithologies with different mechanical
506 properties (Fig. 8). At shallow levels, the landward side of the fault system is mainly composed
507 of stronger, less permeable and porous underplated and accreted metamorphosed and igneous
508 rocks, such as the Ghost Rocks Formation, the Kodiak Formation, igneous plutons, and the late
509 Triassic to early Jurassic accretionary complex. The trenchward side of the fault system is
510 mainly composed of weaker, more permeable and porous accreted rocks that offscraped from the
511 subduction plate represented by the Sitkalidak Formation and younger units (Moore and
512 Allwardt, 1980; Byrne and Fisher, 1987). The first-order across-fault lithology and mechanical
513 property changes are also exhibited by a low seismically-determined V_p/V_s ratio on the arcward
514 side of the island and an increased V_p/V_s ratio on the trenchward side, where the higher V_p/V_s
515 values are usually interpreted as indicative of elevated fluid content (Wang et al., 2024). The
516 strong contrast in mechanical properties is also suggested by across-strike changes in seismic
517 velocity, gravity and magnetic field data (Song and Simons, 2003; Wells et al., 2003; Ramos et
518 al., 2022; Wang et al., 2024).

519 At depths beneath the Kodiak Islands, our estimated fault flat geometry of the Kodiak
520 Shelf Fault is located approximately where there is a high gradient in the seismically-determined
521 V_p/V_s ratio at depths of about 15-20 km within the wedge (Fig. 8). Because the duplex structure
522 may have developed through the mainly Eocene-Oligocene underplating process beneath the
523 Kodiak Islands, the change in V_p/V_s ratio may represent the roof of the duplex structure, i.e., the
524 contact between the underplated material and the stronger, less permeable and less porous
525 metamorphosed and igneous rocks exposed at the surface. The low porosity-permeability rocks,
526 suggested by low V_p/V_s values in the upper crustal part of the wedge may have facilitated the

527 trapping of fluids released from the dehydration of the subducting slab within the underplated
528 rocks, which are characterized by high V_p/V_s values. On the EDGE deep seismic reflection
529 image, approximately 100 km northeast of the Kodiak Islands, a deep arch-shaped high-to-low
530 transition of seismic velocity similar to the large V_p/V_s ratio change in the Kodiak Islands area
531 has been identified and interpreted as the top of the low-velocity underplated material (Fig. 8;
532 Moore et al., 1991; Ye et al., 1997). Therefore, although speculative, it is possible that the flat
533 part of the Kodiak Shelf Fault Zone was developed by exploiting the shear zones of the old
534 duplex system, including the roof thrust. The process might have been facilitated by fluid-
535 influenced mechanical property contrast. The linkage between a similar forearc splay fault and a
536 duplex structure along the subduction interface was suggested based on the seismic images in
537 Prince William Sound, about 300 km northeast along-strike (Haeussler et al., 2015).

538 Previous studies suggest that the interface coupling pattern and seismic behavior along
539 the subduction interface may have been significantly affected by fluid distribution because of its
540 influence on pore-fluid pressure and rheology (e.g. Shillington et al., 2015; Li et al., 2018; Fisher
541 and Hirth, 2024; Wang et al., 2024). Given the coincidence between the inferred Kodiak Shelf
542 Fault geometry and the V_p/V_s pattern (Wang et al., 2024), we envision that the lithology-
543 influenced forearc fluid distribution may have facilitated the long-term continuous deformation
544 along the Kodiak Shelf Fault. Once the splay fault system was established, its damage zone may
545 function as a fluid conduit for releasing the fluid trapped beneath the low porosity-permeability
546 rocks exposed on the Kodiak Islands. Although there is no direct evidence of the process along
547 this offshore fault system, a fluid-rich damage zone has been reported along an ancient out-of-
548 sequence thrust, Uganik Thrust, on the Kodiak Islands (Rowe et al., 2009). The fluid saturation

549 along the fault system can significantly reduce the yield strength and facilitate persistent long-
550 term fault activity.

551 Because the shallow portion of the KSFZ lies above the approximate locked-creeping
552 boundary of the megathrust, earthquakes along the KSFZ may be triggered by upper-plate stress
553 changes during megathrust events. If our predicted fault geometry is correct, the KSFZ could
554 also rupture independently in upper-plate earthquakes without major megathrust earthquakes.

555 **6. Conclusions**

556 Most of our ZHe ages record cooling through ZHe closure temperature in the late
557 Eocene-early Oligocene, and are temporally and spatially consistent with the Eocene-early
558 Oligocene broad antiformal exhumation previously documented by zircon and apatite fission
559 track thermochronological ages. However, our AHe ages reveal a new pattern; the ages record
560 cooling through the AHe closure temperature from early Miocene to Pliocene and exhibit an
561 overall decrease trenchward, with Pliocene ages (3-5 Ma) collected from the trenchward coastal
562 area of the Kodiak Islands. Our thermal history modeling suggests that the trenchward coastal
563 area of the Kodiak Islands experienced a change from early-middle Miocene basin subsidence to
564 recent deformation and rapid uplift since 6-7 Ma. In contrast, the rest of the island experienced
565 an early-middle Miocene transition from the prolonged relatively rapid Eocene-Oligocene
566 exhumation to a slow exhumation phase starting approximately in the late Miocene. The early-
567 middle Miocene change in the exhumation pattern might be caused by a change in the dominant
568 deformation mechanism affecting the Kodiak Islands, from broad underplating along the
569 subduction interface to the hanging-wall uplift of the Kodiak Shelf Fault Zone, an active crustal
570 splay fault system above the down-dip edge of the seismogenic zone. The observation that the
571 newly revealed post-Miocene long-term exhumation pattern resembles the estimated uplift

572 patterns based on elevated Pleistocene marine terraces and decadal geodetic data suggests that
573 the splay-fault-related exhumation has persisted from Miocene to Recent. The inherited upper-
574 plate structures and lithologic architecture may affect the fluid distribution (and possibly pore
575 fluid pressure), and therefore effective rock strength in the forearc wedge in a way that facilitates
576 the development of the Kodiak Shelf Fault and its persistent deformation over geological time.

577

578 **Acknowledgements.** This work was primarily funded by NSF grant EAR-2046278 to K. Morell.
579 The authors are grateful to P. Hauessler for his insight in this work. The authors thank Fan Wang
580 for providing the high-resolution profile of Vp/Vs data (Wang et al., 2024) used in Figure 8. The
581 authors also thank J. Metcalf (CU TRaIL) and A. Kylander-Clark (UC Santa Barbara) for their
582 help with the zircon and apatite (U-Th)/He dating and zircon U-Pb dating analyses, respectively.
583 The authors thank Donna Shillington and Eva Enkelmann for their comments and suggestions
584 that improved the manuscript.

585

586 **References**

- 587 Barker, D. H. N., Henrys, S., Caratori Tontini, F., Barnes, P. M., Bassett, D., Todd, E., and
588 Wallace, L., 2018, Geophysical Constraints on the Relationship Between Seamount
589 Subduction, Slow Slip, and Tremor at the North Hikurangi Subduction Zone, New
590 Zealand: Geophysical Research Letters, v. 45, no. 23,
591 <https://doi.org/10.1029/2018gl080259>.
- 592 Barnes, P. M., Wallace, L. M., Saffer, D. M., Bell, R. E., Underwood, M. B., Fagereng, A.,
593 Meneghini, F., Savage, H. M., Rabinowitz, H. S., Morgan, J. K., Kitajima, H., Kutterolf,
594 S., Hashimoto, Y., Engelmann de Oliveira, C. H., Noda, A., Crundwell, M. P., Shepherd,

595 C. L., Woodhouse, A. D., Harris, R. N., Wang, M., Henrys, S., Barker, D. H. N.,
596 Petronotis, K. E., Bourlange, S. M., Clennell, M. B., Cook, A. E., Dugan, B. E., Elger, J.,
597 Fulton, P. M., Gamboa, D., Greve, A., Han, S., Hüpers, A., Ikari, M. J., Ito, Y., Kim, G.
598 Y., Koge, H., Lee, H., Li, X., Luo, M., Malie, P. R., Moore, G. F., Mountjoy, J. J.,
599 McNamara, D. D., Paganoni, M., Sreaton, E. J., Shankar, U., Shreedharan, S., Solomon,
600 E. A., Wang, X., Wu, H.-Y., Pecher, I. A., and LeVay, L. J., 2020, Slow slip source
601 characterized by lithological and geometric heterogeneity: *Science Advances*, v. 6, no.
602 13, p. eaay3314, <https://doi.org/10.1126/sciadv.aay3314>.

603 Burns, L. E., 1985, The Border Ranges ultramafic and mafic complex, south-central Alaska:
604 cumulate fractionates of island-arc volcanics: *Canadian Journal of Earth Sciences*, v. 22,
605 no. 7, p. 1020-1038, <https://doi.org/10.1139/e85-106>.

606 Byrne, T., 1984, Early deformation in melange terranes of the Ghost Rocks Formation, Kodiak
607 Islands, Alaska, *in* Raymond, L. A., ed., *Melanges: Their Nature, Origin, and*
608 *Significance*, Volume 198, Geological Society of America, p. 21-51,
609 <https://doi.org/10.1130/SPE198-p21>.

610 Byrne, T., 1986, Eocene underplating along the Kodiak Shelf, Alaska: Implications and regional
611 correlations: *Tectonics*, v. 5, no. 3, p. 403-421,
612 <https://doi.org/https://doi.org/10.1029/TC005i003p00403>.

613 Byrne, T., and Fisher, D., 1987, Episodic growth of the Kodiak convergent margin: *Nature*, v.
614 325, no. 6102, p. 338-341, <https://doi.org/10.1038/325338a0>.

615 Carden, J. R., Connelly, W., Forbes, R. B., and Turner, D. L., 1977, Blueschists of the Kodiak
616 Islands, Alaska: An extension of the Seldovia schist terrane: *Geology*, v. 5, no. 9, p. 529-
617 533, [https://doi.org/10.1130/0091-7613\(1977\)5](https://doi.org/10.1130/0091-7613(1977)5)<529:Botkia>2.0.Co;2.

618 Carver, G., Sauber, J., Lettis, W., Witter, R., Whitney, B., and Freymueller, J., 2008, Active
619 faults on northeastern Kodiak Island, Alaska: Active tectonics and seismic potential of
620 Alaska: American Geophysical Union Geophysical Monograph, v. 179, p. 167-184.

621 Clendenen, W. S., Fisher, D., Byrne, T., Sisson, V. B., Roeske, S. M., and Pavlis, T. L., 2003,
622 Cooling and exhumation history of the Kodiak accretionary prism, southwest Alaska, *in*
623 Sisson, V. B., Roeske, S. M., and Pavlis, T. L., eds., Geology of a transpressional orogen
624 developed during ridge-trench interaction along the North Pacific margin, Volume 371:
625 Boulder, Colorado, Geological Society of America Special Paper 371, p. 71-88,
626 <https://doi.org/10.1130/0-8137-2371-x.71>.

627 Clendenen, W. S., Sliter, W. V., and Byrne, T., 1992, Tectonic implications of the Albatross
628 sedimentary sequence, Sitkinak Island, Alaska.

629 Connelly, W., 1978, Uyak Complex, Kodiak Islands, Alaska: A Cretaceous subduction complex:
630 GSA Bulletin, v. 89, no. 5, p. 755-769, [https://doi.org/10.1130/0016-7606\(1978\)89<755:UCKIAA>2.0.CO;2](https://doi.org/10.1130/0016-7606(1978)89<755:UCKIAA>2.0.CO;2).

631

632 Cook, B. J., Henstock, T. J., McNeill, L. C., and Bull, J. M., 2014, Controls on spatial and
633 temporal evolution of prism faulting and relationships to plate boundary slip offshore
634 north-central Sumatra: Journal of Geophysical Research: Solid Earth, v. 119, no. 7, p.
635 5594-5612, <https://doi.org/10.1002/2013jb010834>.

636 Cummins, P. R., and Kaneda, Y., 2000, Possible splay fault slip during the 1946 Nankai
637 earthquake: Geophysical Research Letters, v. 27, no. 17, p. 2725-2728,
638 <https://doi.org/https://doi.org/10.1029/1999GL011139>.

639 Davies, J., Sykes, L., House, L., and Jacob, K., 1981, Shumagin Seismic Gap, Alaska Peninsula -
640 History of Great Earthquakes, Tectonic Setting, and Evidence for High Seismic Potential:

641 Journal of Geophysical Research, v. 86, no. Nb5, p. 3821-3855,
642 <https://doi.org/10.1029/JB086iB05p03821>.

643 DeMets, C., Gordon, R. G., Argus, D. F., and Stein, S., 1990, Current plate motions:
644 Geophysical Journal International, v. 101, no. 2, p. 425-478,
645 <https://doi.org/10.1111/j.1365-246X.1990.tb06579.x>.

646 DePaolis, J. M., Dura, T., Witter, R. C., Haeussler, P. J., Bender, A., Curran, J. H., and Corbett,
647 D. R., 2024, Repeated Coseismic Uplift of Coastal Lagoons Above the Patton Bay Splay
648 Fault System, Montague Island, Alaska, USA: Journal of Geophysical Research: Solid
649 Earth, v. 129, no. 5, <https://doi.org/10.1029/2023jb028552>.

650 Dielforder, A., Hetzel, R., and Oncken, O., 2020, Megathrust shear force controls mountain
651 height at convergent plate margins: Nature, v. 582, no. 7811, p. 225-229,
652 <https://doi.org/10.1038/s41586-020-2340-7>.

653 Elliott, J., and Freymueller, J. T., 2020, A Block Model of Present-Day Kinematics of Alaska
654 and Western Canada: Journal of Geophysical Research: Solid Earth, v. 125, no. 7, p.
655 e2019JB018378, <https://doi.org/10.1029/2019JB018378>.

656 Farris, D. W., 2010, Tectonic and petrologic evolution of the Kodiak batholith and the
657 trenchward belt, Kodiak Island, AK: Contact fault juxtaposition?: Journal of Geophysical
658 Research, v. 115, no. B7, <https://doi.org/10.1029/2009jb006434>.

659 Farris, D. W., Haeussler, P., Friedman, R., Paterson, S. R., Saltus, R. W., and Ayuso, R., 2006,
660 Emplacement of the Kodiak batholith and slab-window migration: Geological Society of
661 America Bulletin, v. 118, no. 11-12, p. 1360-1376, <https://doi.org/10.1130/b25718.1>.

662 Fisher, D., and Byrne, T., 1987, Structural evolution of underthrust sediments, Kodiak Islands,
663 Alaska: Tectonics, v. 6, no. 6, p. 775-793, <https://doi.org/10.1029/TC006i006p00775>.

664 Fisher, D. M., and Byrne, T., 1992, Strain variations in an ancient accretionary complex:
665 Implications for forearc evolution: *Tectonics*, v. 11, no. 2, p. 330-347,
666 <https://doi.org/10.1029/91tc01490>.

667 Fisher, D. M., and Hirth, G., 2024, A pressure solution flow law for the seismogenic zone:
668 Application to Cascadia: *Science Advances*, v. 10, no. 4, p. eadi7279,
669 <https://doi.org/doi:10.1126/sciadv.adi7279>.

670 Fisher, D. M., Tonai, S., Hashimoto, Y., Tomioka, N., and Oakley, D., 2019, K-Ar Dating of
671 Fossil Seismogenic Thrusts in the Shimanto Accretionary Complex, Southwest Japan:
672 *Tectonics*, v. 38, no. 11, p. 3866-3880,
673 <https://doi.org/https://doi.org/10.1029/2019TC005571>.

674 Fisher, M. A., and Holmes, M. L., 1980, Large-scale structure of deep strata beneath Kodiak
675 shelf, Alaska: *GSA Bulletin*, v. 91, no. 4, p. 218-224, [https://doi.org/10.1130/0016-](https://doi.org/10.1130/0016-7606(1980)91<218:Lsodsb>2.0.Co;2)
676 [7606\(1980\)91<218:Lsodsb>2.0.Co;2](https://doi.org/10.1130/0016-7606(1980)91<218:Lsodsb>2.0.Co;2).

677 Flowers, R. M., Ketcham, R. A., Shuster, D. L., and Farley, K. A., 2009, Apatite (U–Th)/He
678 thermochronometry using a radiation damage accumulation and annealing model:
679 *Geochimica et Cosmochimica Acta*, v. 73, no. 8, p. 2347-2365,
680 <https://doi.org/10.1016/j.gca.2009.01.015>.

681 Haeussler, P. J., Armstrong, P. A., Liberty, L. M., Ferguson, K. M., Finn, S. P., Arkle, J. C., and
682 Pratt, T. L., 2015, Focused exhumation along megathrust splay faults in Prince William
683 Sound, Alaska: *Quaternary Science Reviews*, v. 113, p. 8-22,
684 <https://doi.org/10.1016/j.quascirev.2014.10.013>.

685 Haeussler, P. J., Bradley, D. C., Wells, R. E., and Miller, M. L., 2003, Life and death of the
686 Resurrection plate: Evidence for its existence and subduction in the northeastern Pacific

687 in Paleocene–Eocene time: GSA Bulletin, v. 115, no. 7, p. 867-880,
688 [https://doi.org/10.1130/0016-7606\(2003\)115<0867:Ladotr>2.0.Co;2](https://doi.org/10.1130/0016-7606(2003)115<0867:Ladotr>2.0.Co;2).

689 Hayes, G. P., Moore, G. L., Portner, D. E., Hearne, M., Flamme, H., Furtney, M., and Smoczyk,
690 G. M., 2018, Slab2, a comprehensive subduction zone geometry model: Science, v. 362,
691 no. 6410, p. 58-61, <https://doi.org/10.1126/science.aat4723>.

692 Jolivet, R., Simons, M., Duputel, Z., Olive, J.-A., Bhat, H. S., and Bletery, Q., 2020, Interseismic
693 Loading of Subduction Megathrust Drives Long-Term Uplift in Northern Chile:
694 Geophysical Research Letters, v. 47, no. 8, p. e2019GL085377,
695 <https://doi.org/10.1029/2019gl085377>.

696 Ketcham, R. A., 2005, Forward and Inverse Modeling of Low-Temperature Thermochronometry
697 Data: Reviews in Mineralogy and Geochemistry, v. 58, no. 1, p. 275-314,
698 <https://doi.org/10.2138/rmg.2005.58.11>.

699 Kimura, G., Kitamura, Y., Hashimoto, Y., Yamaguchi, A., Shibata, T., Ujiie, K., and Okamoto,
700 S. y., 2007, Transition of accretionary wedge structures around the up-dip limit of the
701 seismogenic subduction zone: Earth and Planetary Science Letters, v. 255, no. 3, p. 471-
702 484, <https://doi.org/https://doi.org/10.1016/j.epsl.2007.01.005>.

703 Li, J., Shillington, D. J., Saffer, D. M., Bécel, A., Nedimović, M. R., Kuehn, H., Webb, S. C.,
704 Keranen, K. M., and Abers, G. A., 2018, Connections between subducted sediment, pore-
705 fluid pressure, and earthquake behavior along the Alaska megathrust: Geology, v. 46, no.
706 4, p. 299-302, <https://doi.org/10.1130/g39557.1>.

707 Liberty, L. M., Brothers, D. S., and Haeussler, P. J., 2019, Tsunamigenic Splay Faults Imply a
708 Long-Term Asperity in Southern Prince William Sound, Alaska: Geophysical Research
709 Letters, v. 46, no. 7, p. 3764-3772, <https://doi.org/10.1029/2018gl081528>.

710 Liberty, L. M., Finn, S. P., Haeussler, P. J., Pratt, T. L., and Peterson, A., 2013, Megathrust splay
711 faults at the focus of the Prince William Sound asperity, Alaska: *Journal of Geophysical*
712 *Research: Solid Earth*, v. 118, no. 10, p. 5428-5441, <https://doi.org/10.1002/jgrb.50372>.

713 Liu, C., Lay, T., and Xiong, X., 2022, The 29 July 2021 M-W 8.2 Chignik, Alaska Peninsula
714 Earthquake Rupture Inferred From Seismic and Geodetic Observations: Re-Rupture of
715 the Western 2/3 of the 1938 Rupture Zone: *Geophysical Research Letters*, v. 49, no. 4,
716 <https://doi.org/10.1029/2021gl096004>.

717 Marinovich, L., Jr, and Moriya, S., 1992, Early middle Miocene mollusks and benthic
718 foraminifers from Kodiak Island, Alaska.

719 Michel-Wolf, L., Ehlers, T. A., and Bendick, R., 2022, Transitions in subduction zone properties
720 align with long-term topographic growth (Cascadia, USA): *Earth and Planetary Science*
721 *Letters*, v. 580, <https://doi.org/10.1016/j.epsl.2021.117363>.

722 Moore, G. F., Bangs, N. L., Taira, A., Kuramoto, S., Pangborn, E., and Tobin, H. J., 2007,
723 Three-Dimensional Splay Fault Geometry and Implications for Tsunami Generation:
724 *Science*, v. 318, no. 5853, p. 1128-1131, <https://doi.org/doi:10.1126/science.1147195>.

725 Moore, J. C., 1978, Orientation of underthrusting during latest Cretaceous and earliest Tertiary
726 time, Kodiak Islands, Alaska: *Geology*, v. 6, no. 4, p. 209-213,
727 [https://doi.org/10.1130/0091-7613\(1978\)6<209:Ooudlc>2.0.Co;2](https://doi.org/10.1130/0091-7613(1978)6<209:Ooudlc>2.0.Co;2).

728 Moore, J. C., and Allwardt, A., 1980, Progressive deformation of a Tertiary Trench Slope,
729 Kodiak Islands, Alaska: *Journal of Geophysical Research: Solid Earth*, v. 85, no. B9, p.
730 4741-4756, <https://doi.org/10.1029/JB085iB09p04741>.

731 Moore, J. C., Byrne, T., Plumley, P. W., Reid, M., Gibbons, H., and Coe, R. S., 1983, Paleogene
732 evolution of the Kodiak Islands, Alaska: Consequences of ridge-trench interaction in a

733 more southerly latitude: *Tectonics*, v. 2, no. 3, p. 265-293,
734 <https://doi.org/10.1029/TC002i003p00265>.

735 Moore, J. C., Diebold, J., Fisher, M. A., Sample, J., Brocher, T., Talwani, M., Ewing, J., Huene,
736 R. v., Rowe, C., Stone, D., Stevens, C., and Sawyer, D., 1991, EDGE deep seismic
737 reflection transect of the eastern Aleutian arc-trench layered lower crust reveals
738 underplating and continental growth: *Geology*, v. 19, no. 5, p. 420-424,
739 [https://doi.org/10.1130/0091-7613\(1991\)019<0420:EDSRTO>2.3.CO;2](https://doi.org/10.1130/0091-7613(1991)019<0420:EDSRTO>2.3.CO;2) %J *Geology*.

740 Nilsen, T. H., and Moore, G. W., 1979, Reconnaissance study of Upper Cretaceous to Miocene
741 stratigraphic units and sedimentary facies, Kodiak and adjacent islands, Alaska, with a
742 section on sedimentary petrography.

743 Oryan, B., Olive, J.-A., Jolivet, R., Malatesta, L. C., Gailleton, B., and Bruhat, L., 2024,
744 Megathrust locking encoded in subduction landscapes: *Science Advances*, v. 10, no. 17,
745 p. ead14286, <https://doi.org/doi:10.1126/sciadv.adl4286>.

746 Park, J.-O., Tsuru, T., Kodaira, S., Cummins, P. R., and Kaneda, Y., 2002, Splay Fault
747 Branching Along the Nankai Subduction Zone: *Science*, v. 297, no. 5584, p. 1157-1160,
748 <https://doi.org/doi:10.1126/science.1074111>.

749 Plafker, G., 1965, Tectonic Deformation Associated with the 1964 Alaska Earthquake: *Science*,
750 v. 148, no. 3678, p. 1675-1687, <https://doi.org/doi:10.1126/science.148.3678.1675>.

751 Qin, Y., Chen, J., Singh, S. C., Hananto, N., Carton, H., and Tapponnier, P., 2024, Assessing the
752 Risk of Potential Tsunamigenic Earthquakes in the Mentawai Region by Seismic
753 Imaging, Central Sumatra: *Geochemistry, Geophysics, Geosystems*, v. 25, no. 5,
754 <https://doi.org/10.1029/2023gc011149>.

755 Rajič, K., Raimbourg, H., Famin, V., Moris-Muttoni, B., Fisher, D. M., Morell, K. D., and
756 Canizarés, A., 2023, Exhuming an Accretionary Prism: A Case Study of the Kodiak
757 Accretionary Complex, Alaska, USA: *Tectonics*, v. 42, no. 10,
758 <https://doi.org/10.1029/2023tc007754>.

759 Ramos, M. D., Liberty, L. M., Haeussler, P. J., and Humphreys, R., 2022, Upper-plate structure
760 and tsunamigenic faults near the Kodiak Islands, Alaska, USA: *Geosphere*, v. 18, no. 5,
761 p. 1474-1491, <https://doi.org/10.1130/ges02486.1>.

762 Reiners, P. W., 2005, Zircon (U-Th)/He Thermochronometry: Reviews in Mineralogy and
763 Geochemistry, v. 58, no. 1, p. 151-179, <https://doi.org/10.2138/rmg.2005.58.6>.

764 Reiners, P. W., Spell, T. L., Nicolescu, S., and Zanetti, K. A., 2004, Zircon (U-Th)/He
765 thermochronometry: He diffusion and comparisons with $^{40}\text{Ar}/^{39}\text{Ar}$ dating: *Geochimica*
766 *et Cosmochimica Acta*, v. 68, no. 8, p. 1857-1887,
767 <https://doi.org/10.1016/j.gca.2003.10.021>.

768 Roeske, S. M., Mattinson, J. M., and Armstrong, R. L., 1989, Isotopic ages of glaucophane
769 schists on the Kodiak Islands, southern Alaska, and their implications for the Mesozoic
770 tectonic history of the Border Ranges fault system: *Geological Society of America*
771 *Bulletin*, v. 101, no. 8, p. 1021-1037, [https://doi.org/10.1130/0016-
772 7606\(1989\)101<1021:IAOGSO>2.3.CO;2](https://doi.org/10.1130/0016-7606(1989)101<1021:IAOGSO>2.3.CO;2).

773 Rowe, C. D., Meneghini, F., and Moore, J. C., 2009, Fluid-rich damage zone of an ancient out-
774 of-sequence thrust, Kodiak Islands, Alaska: *Tectonics*, v. 28, no. 1,
775 <https://doi.org/10.1029/2007TC002126>.

776 Saillard, M., Audin, L., Rousset, B., Avouac, J.-P., Chlieh, M., Hall, S. R., Husson, L., and
777 Farber, D. L., 2017, From the seismic cycle to long-term deformation: linking seismic

778 coupling and Quaternary coastal geomorphology along the Andean megathrust:
779 Tectonics, v. 36, no. 2, p. 241-256, <https://doi.org/doi:10.1002/2016TC004156>.

780 Sample, J. C., and Fisher, D. M., 1986, Duplex accretion and underplating in an ancient
781 accretionary complex, Kodiak Islands, Alaska: Geology, v. 14, no. 2, p. 160-163,
782 [https://doi.org/10.1130/0091-7613\(1986\)14<160:Daauia>2.0.Co;2](https://doi.org/10.1130/0091-7613(1986)14<160:Daauia>2.0.Co;2).

783 Sample, J. C., and Moore, J. C., 1987, Structural style and kinematics of an underplated slate
784 belt, Kodiak and adjacent islands, Alaska: GSA Bulletin, v. 99, no. 1, p. 7-20,
785 [https://doi.org/10.1130/0016-7606\(1987\)99<7:Ssako>2.0.Co;2](https://doi.org/10.1130/0016-7606(1987)99<7:Ssako>2.0.Co;2).

786 Sample, J. C., and Reid, M. R., 2003, Large-scale, latest Cretaceous uplift along the Northeast
787 Pacific Rim: Evidence from sediment volume, sandstone petrography, and Nd isotope
788 signatures of the Kodiak Formation, Kodiak Islands, Alaska, *in* Sisson, V. B., Roeske, S.
789 M., and Pavlis, T. L., eds., Geology of a transpressional orogen developed during ridge-
790 trench interaction along the North Pacific margin, Volume 371, Geological Society of
791 America, p. 0, <https://doi.org/10.1130/0-8137-2371-x.51>.

792 Sauber, J., Carver, G., Cohen, S., and King, R., 2006, Crustal deformation and the seismic cycle
793 across the Kodiak Islands, Alaska: Journal of Geophysical Research: Solid Earth, v. 111,
794 no. B2, <https://doi.org/10.1029/2005JB003626>.

795 Shillington, D. J., Bécel, A., Nedimović, M. R., Kuehn, H., Webb, S. C., Abers, G. A., Keranen,
796 K. M., Li, J., Delescluse, M., and Mattei-Salicrup, G. A., 2015, Link between plate
797 fabric, hydration and subduction zone seismicity in Alaska: Nature Geoscience, v. 8, no.
798 12, p. 961-964, <https://doi.org/10.1038/ngeo2586>.

799 Sibuet, J., Rangin, C., Lepichon, X., Singh, S., Cattaneo, A., Graindorge, D., Klingelhoefer, F.,
800 Lin, J., Malod, J., and Maury, T., 2007, 26th December 2004 great Sumatra–Andaman

801 earthquake: Co-seismic and post-seismic motions in northern Sumatra: Earth and
802 Planetary Science Letters, v. 263, no. 1-2, p. 88-103,
803 <https://doi.org/10.1016/j.epsl.2007.09.005>.

804 Song, T.-R. A., and Simons, M., 2003, Large Trench-Parallel Gravity Variations Predict
805 Seismogenic Behavior in Subduction Zones: Science, v. 301, no. 5633, p. 630-633,
806 <https://doi.org/10.1126/science.1085557>.

807 Strasser, M., Moore, G. F., Kimura, G., Kitamura, Y., Kopf, A. J., Lallemand, S., Park, J.-O.,
808 Sreaton, E. J., Su, X., Underwood, M. B., and Zhao, X., 2009, Origin and evolution of a
809 splay fault in the Nankai accretionary wedge: Nature Geoscience, v. 2, no. 9, p. 648-652,
810 <https://doi.org/10.1038/ngeo609>.

811 Suito, H., and Freymueller, J. T., 2009, A viscoelastic and afterslip postseismic deformation
812 model for the 1964 Alaska earthquake: Journal of Geophysical Research: Solid Earth, v.
813 114, no. B11, <https://doi.org/10.1029/2008jb005954>.

814 Suleimani, E., and Freymueller, J. T., 2020, Near-Field Modeling of the 1964 Alaska Tsunami:
815 The Role of Splay Faults and Horizontal Displacements: Journal of Geophysical
816 Research: Solid Earth, v. 125, no. 7, <https://doi.org/10.1029/2020jb019620>.

817 van der Beek, P., and Schildgen, T. F., 2023, Short communication: age2exhume – a
818 MATLAB/Python script to calculate steady-state vertical exhumation rates from
819 thermochronometric ages and application to the Himalaya: Geochronology, v. 5, no. 1, p.
820 35-49, <https://doi.org/10.5194/gchron-5-35-2023>.

821 van Zelst, I., Rannabauer, L., Gabriel, A. A., and van Dinther, Y., 2022, Earthquake Rupture on
822 Multiple Splay Faults and Its Effect on Tsunamis: Journal of Geophysical Research:
823 Solid Earth, v. 127, no. 8, <https://doi.org/10.1029/2022jb024300>.

824 von Huene, R., Miller, J. J., and Krabbenhoft, A., 2021, The Alaska Convergent Margin
825 Backstop Splay Fault Zone, a Potential Large Tsunami Generator Between the Frontal
826 Prism and Continental Framework: *Geochemistry, Geophysics, Geosystems*, v. 22, no. 1,
827 p. e2019GC008901, <https://doi.org/10.1029/2019GC008901>.

828 Wang, F., Wei, S. S., Drooff, C., Elliott, J. L., Freymueller, J. T., Ruppert, N. A., and Zhang, H.,
829 2024, Fluids control along-strike variations in the Alaska megathrust slip: *Earth and*
830 *Planetary Science Letters*, v. 633, <https://doi.org/10.1016/j.epsl.2024.118655>.

831 Wang, K., and Hu, Y., 2006, Accretionary prisms in subduction earthquake cycles: The theory of
832 dynamic Coulomb wedge: *Journal of Geophysical Research: Solid Earth*, v. 111, no. B6,
833 <https://doi.org/10.1029/2005jb004094>.

834 Wang, X., and Morgan, J., 2022, Effects of coseismic megasplay fault activity on earthquake
835 hazards: Insights from discrete element simulations: *Journal of Structural Geology*, v.
836 155, <https://doi.org/10.1016/j.jsg.2022.104533>.

837 Wells, R. E., Blakely, R. J., Sugiyama, Y., Scholl, D. W., and Dinterman, P. A., 2003, Basin-
838 centered asperities in great subduction zone earthquakes: A link between slip, subsidence,
839 and subduction erosion?: *Journal of Geophysical Research: Solid Earth*, v. 108, no. B10,
840 <https://doi.org/10.1029/2002jb002072>.

841 Wendt, J., Oglesby, D. D., and Geist, E. L., 2009, Tsunamis and splay fault dynamics:
842 *Geophysical Research Letters*, v. 36, no. 15, p. n/a-n/a,
843 <https://doi.org/10.1029/2009gl038295>.

844 Wilson, F. H., 2013, Reconnaissance geologic map of Kodiak Island and adjacent islands,
845 Alaska: US Geological Survey, scale 1:500,000.

846 Ye, S., Flueh, E. R., Klaeschen, D., and von Huene, R., 1997, Crustal structure along the EDGE
847 transect beneath the Kodiak shelf off Alaska derived from OBH seismic refraction data:
848 Geophysical Journal International, v. 130, no. 2, p. 283-302,
849 <https://doi.org/10.1111/j.1365-246X.1997.tb05648.x>.

850

851

852 **Figure Captions**

853 Fig 1. Geological map of Kodiak Islands area (Wilson, 2013) with sample locations and a subset
854 of the new thermochronology ages. Zircon and apatite (U-Th)/He (ZHe and AHe) ages are new
855 data and their sample names are labeled. Zircon fission track (ZFT) and apatite fission track
856 (AFT) ages are from Clendenen et al. (2003). Age numbers in the same box are from the same
857 sample. Ages within the gray dashed rectangle are shown in Fig. 2. The locked-creeping
858 boundary is based on Elliott and Freymueller (2020). The inset map in the lower-left corner
859 shows the details of a sample cluster. The regional map in the lower-right shows plate
860 boundaries, rupture areas of forearc large earthquakes (circles; Davies et al., 1981; Liu et al.,
861 2022), Quaternary faults (red lines; from U.S. Geological Survey), the main map extent (gray
862 dashed box) and the profile line. Map units: Tnc – Narrow Cape Formation, Tsk – Sitkinak
863 Formation, Tsi – Sitkalidak Formation, TKghm – Ghost Rocks Formation mélange unit, TKghc
864 – Ghost Rocks Formation coherent unit, Kkd – Kodiak Formation, Tin – Paleogene intrusive
865 rocks, Kmk – Uyak Complex, Jsch – Raspberry schist, Trqd – Triassic Afognak pluton, Trs –
866 Triassic sedimentary unit.

867
868 Fig. 2 (a) Geological map of the main sample area with thermochronological ages. Underlined
869 numbers indicate the youngest grain age of the sample. M1-M5 are locations of thermal history
870 models in Fig 6. (b) Detailed map of the Narrow Cape Fm area. Active faults were mapped by
871 Carver et al. (2008). Other map symbols are the same as Fig. 1. (c-d) Field photos show high-
872 angle faults that cut the Narrow Cape Formation and unconformity and stereonet plots of faults,
873 kinematic indicators and bedding at the two localities. (e) A profile along the coastal cliff shows
874 cliff topography, unconformity elevation (black dots are field measurements), sample locations
875 (red stars), and high-angle faults. The topographic profile is extracted along the dotted blue line
876 in (b) and projected to a straight line subparallel to the coast.

877
878 Fig. 3 Bathymetry map (a) and topographic profiles (b-e) show the active Kodiak Shelf Fault
879 Zone. U – up, D – down. Black arrows in b and c indicate topographic scarps. Note that profile
880 P4 has a different scale from profile P1-P3.

881

882 Fig. 4 Thermochronology age profile. The profile starts at the offshore Ugak Fault (Distance =
883 186 km on Fig. 8 profile) and is made along the thick gray dash line in Fig. 1. The zircon and
884 apatite (U-Th)/He (ZHe and AHe) ages are from this study. The zircon and apatite fission track
885 (ZFT and AFT) ages are from Clendenen et al. (2003). The five ZHe samples closest to the Ugak
886 Fault in the dashed gray polygon are not thermally reset for ZHe system after deposition (refer to
887 text for details) and for each of these samples, only the youngest grain age is plotted. AFT ages
888 at about 40 km are from the sample cluster shown in the inset map in Fig. 1. Their ages vary with
889 elevation (see Supplementary Information). Labels M1-M5 represent the approximate locations
890 of the thermal history models along the profile.

891
892 Fig. 5 Probability density plots of detrital zircon U-Pb ages of the Narrow Cape Formation and
893 Sitkalidak Formation. The plots only show the ages younger than 250 Ma, which are the main
894 component of the data. For each sample, N and n are the number of zircons analyzed and the
895 number of ages younger than 250 Ma, respectively. The complete dataset is reported in Table S2.

896
897 Fig. 6 Thermal history modeling results using HeFTy version 1.9.3 (Ketcham, 2005). The
898 modeled locations are shown in Figs. 2 and 4. Constraints in each model are based on geological
899 context, geochronology and thermochronology ages (Supplementary Information), and peak
900 temperature estimations reported by (Rajič et al., 2023).

901
902 Fig. 7 A trench-normal profile of estimated exhumation rates of apatite (U-Th)/He (AHe)
903 samples (crosses) and uplift rates of marine terraces (upper panel) and estimated possible
904 combinations of overall KSFZ fault geometries and slip rates by assuming various frontal dip
905 angles (lower panel). Three sets of exhumation rate estimations assumed an initial geothermal
906 gradient of 25 °C/km, 30 °C/km and 35°C/km (red, black and blue symbols, respectively). Gray
907 shadow represents max-min uncertainties calculated from uncertainties of AHe ages. Marine
908 terrace uplift rates were estimated based on the terrace elevation measurements and age
909 assumption by Carver et al. (2008). Fault geometries and average slip rates were estimated based
910 on the long-term exhumation rate pattern revealed by AHe ages. The profile starts at the offshore
911 Ugak Fault (Distance = 186 km on Fig. 8 profile).

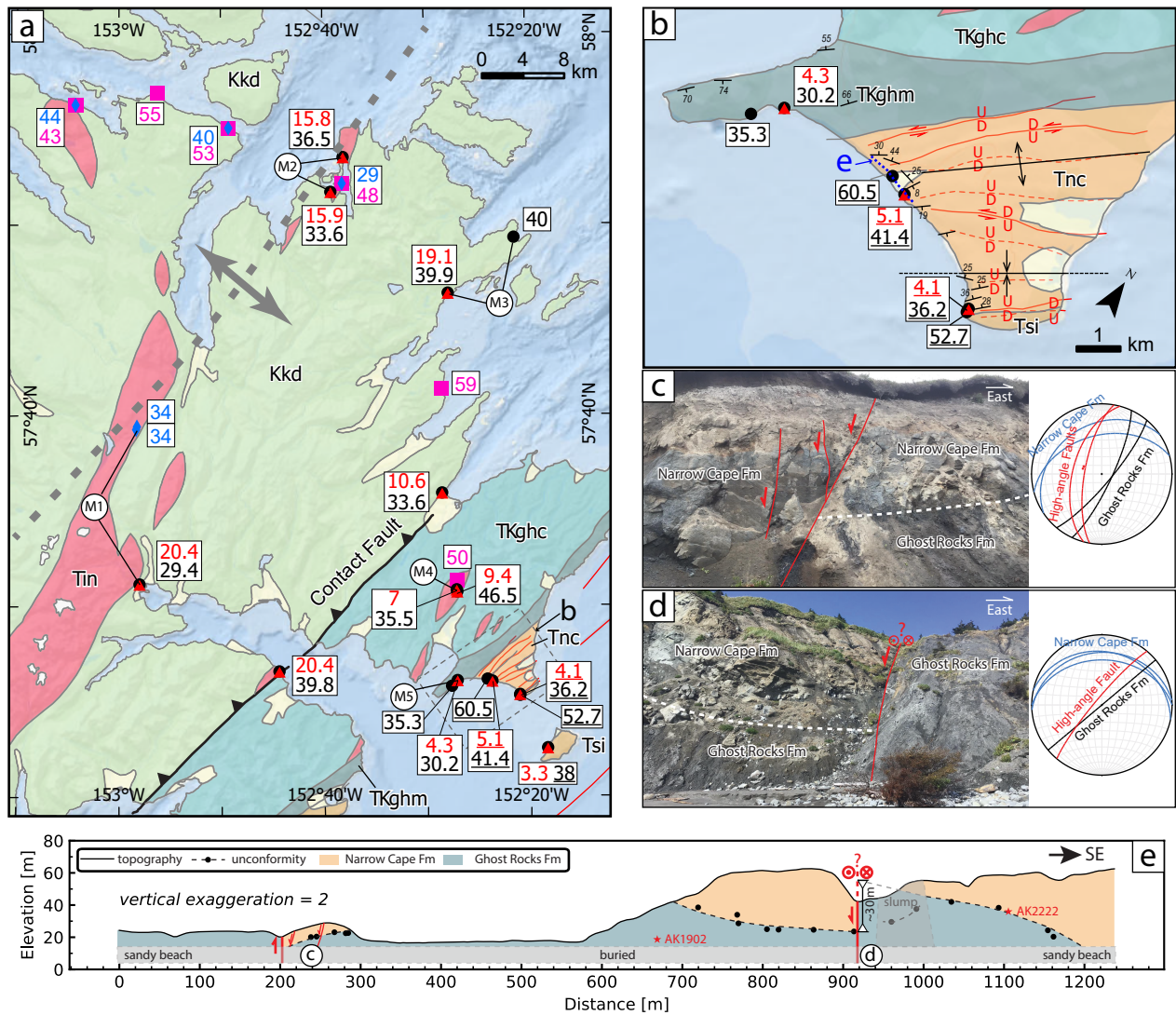
912

913 Fig. 8 A cross-section explaining recent exhumation history and a structural model. The
914 subduction interface geometry is based on Slab 2 (Hayes et al., 2018). The thick gray line is the
915 normal-to-section projection of a major seismic velocity change documented by Ye et al. (1997)
916 on the EDGE transect approximately 100 km northeast of the Kodiak Islands. The upper and
917 lower ends of the locked-creeping transition are interpreted based on the subduction interface
918 coupling coefficient in the Kodiak region reported by Elliot and Freymueller (2020). The up-dip
919 limit of the locked segment is schematic. The grey dashed lines represent the hypothesized
920 structural grain based on the available data. The red lines represent known (solid lines) and
921 schematic (dashed lines) active faults. The Vp/Vs data is along a transect across the Kodiak
922 Islands subparallel to our profile (Wang et al. 2024).

923

924

Figure 2



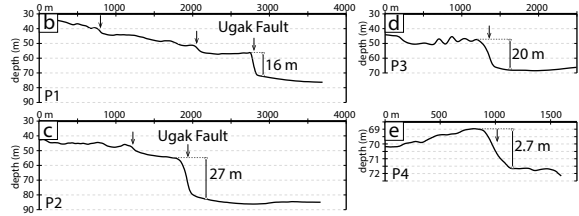
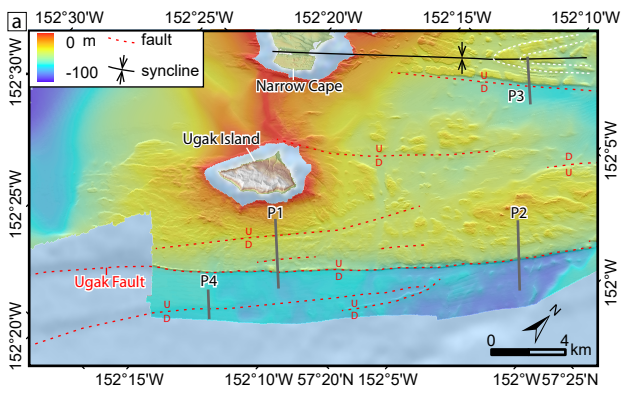
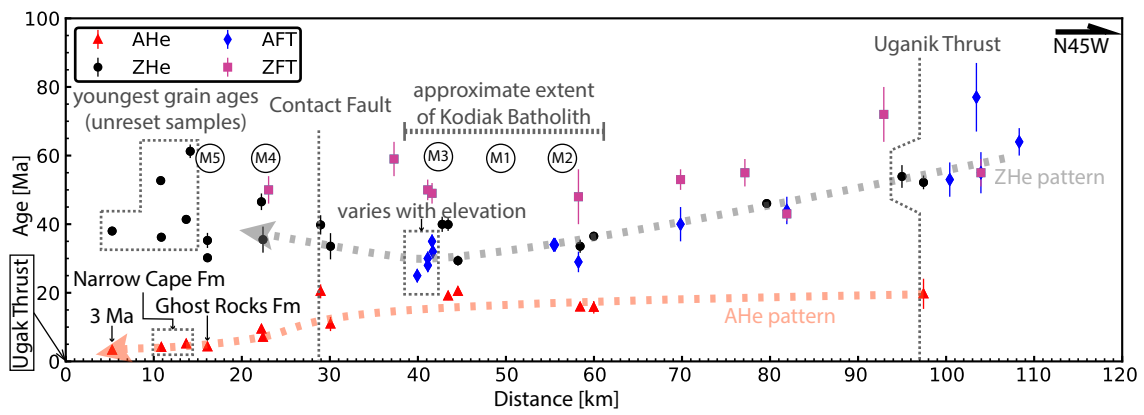
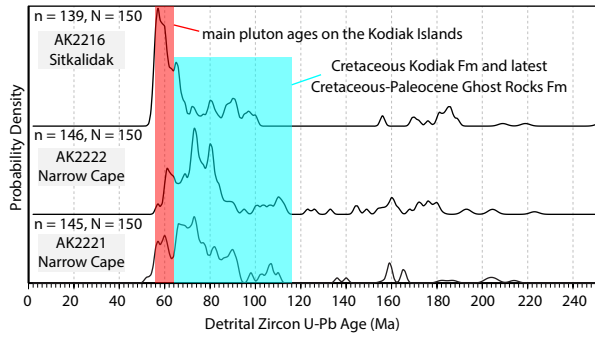
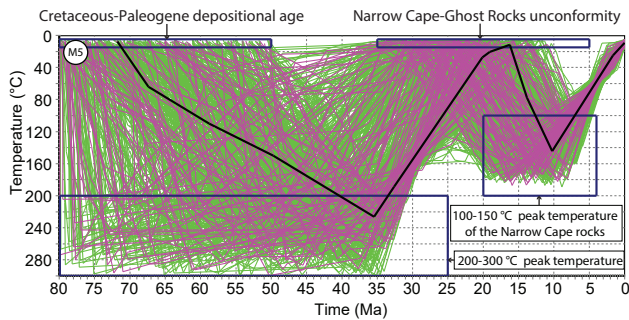
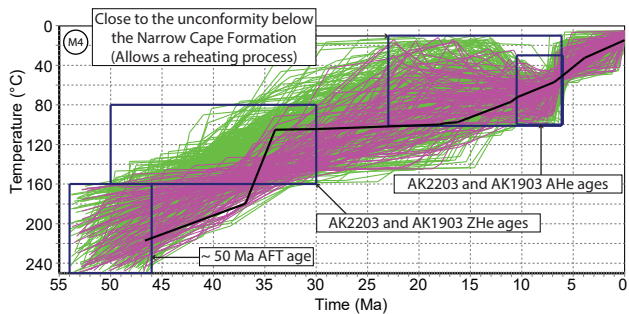
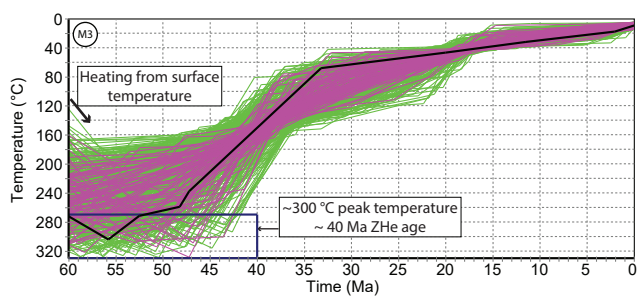
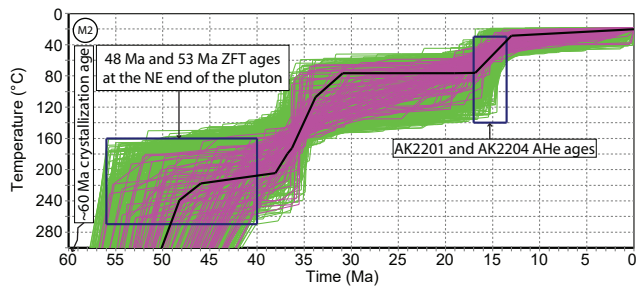
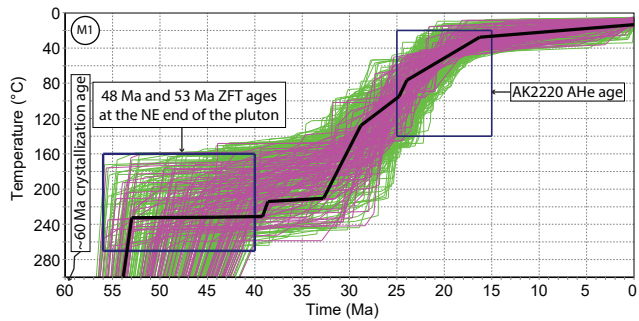


Figure 3

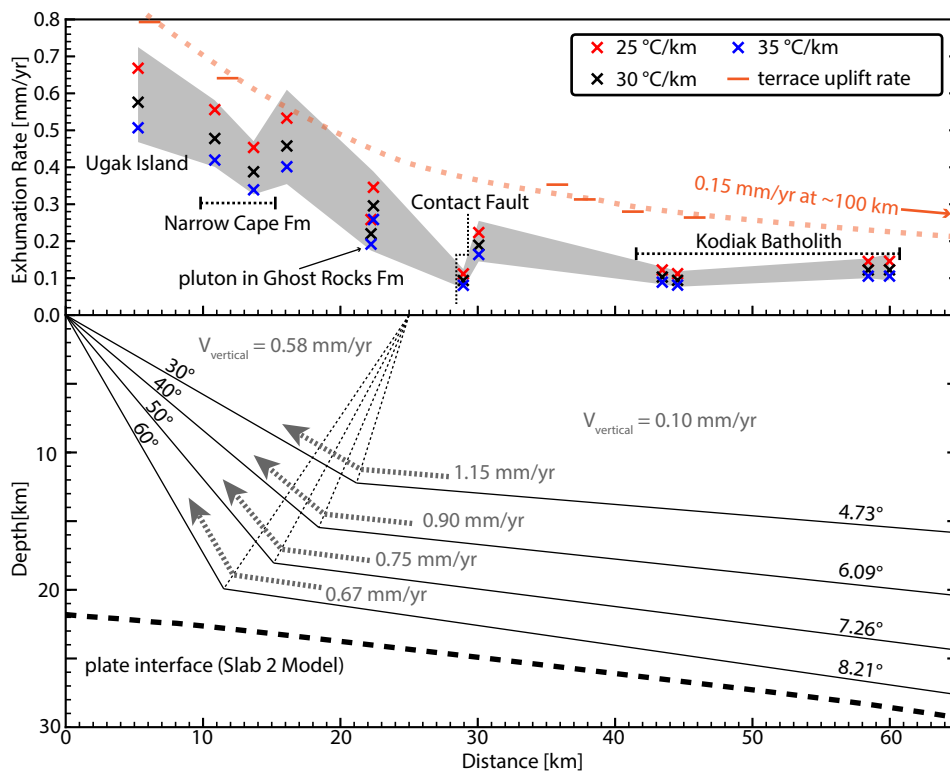






Model fit: — acceptable — good — best

Figure 7



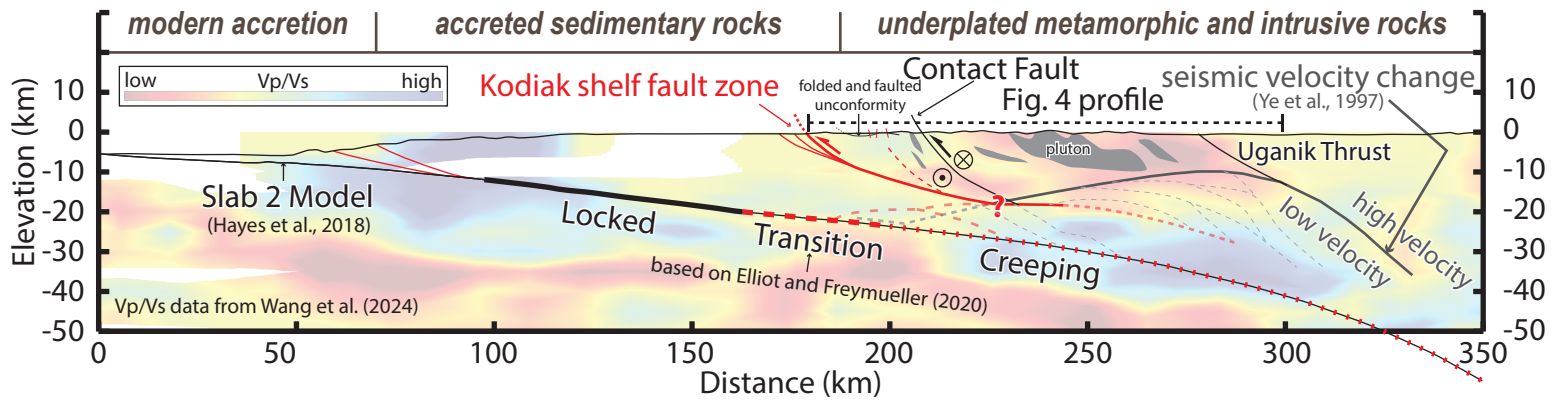


Table 1. Sample information and interpreted thermochronologic ages.

Sample ID	Latitude	Longitude	Elevation (m)	Rock Unit	ZHe (Ma)*	AHe (Ma)*
AK2201	57.862190	-152.653643	7.7	Paleogene Pluton	33.6 ± 1.9	15.9 ± 0.8
AK2203	57.514318	-152.451663	86.1	Paleogene Pluton	35.5 ± 3.8	7.0 ± 0.8
AK2204	57.892507	-152.633262	0.0	Paleogene Pluton	36.5 ± 1.0	15.8 ± 1.8
AK2210	57.599029	-152.474215	28.4	Kodiak Fm.	33.6 ± 3.8	10.6 ± 1.3
AK2211	57.773516	-152.462683	53.6	Kodiak Fm.	39.9 ± 1.9	19.1 ± 1.2
AK2213	57.821888	-152.354314	6.1	Kodiak Fm.	40.0 ± 2.2	-
AK2216	57.375702	-152.306023	0.8	Sitkalidak Fm.	38.0 ± 1.2	3.3 ± 0.3
AK2218	57.443505	-152.73995	9.8	Paleogene Pluton	39.8 ± 2.8	20.4 ± 2.0
AK2220	57.519658	-152.966643	19.1	Paleogene Pluton	29.4 ± 1.5	20.4 ± 1.1
AK2222	57.434397	-152.395072	12.1	Narrow Cape Fm.	41.4 ± 1.2	<i>5.1 ± 0.2</i>
AK2224	57.421713	-152.350214	8.7	Narrow Cape Fm.	52.7 ± 1.2	-
AK2225	57.422501	-152.350341	21.6	Narrow Cape Fm.	36.2 ± 0.8	<i>4.1 ± 0.2</i>
AK2228	57.435045	-152.451337	23.2	Ghost Rock Fm.	30.2 ± 0.7	4.3 ± 0.6
AK1901	57.430151	-152.460473	23.2	Ghost Rock Fm.	35.3 ± 2.2	-
AK1902	57.436105	-152.402721	12.1	Ghost Rock Fm.	60.5 ± 2.4	-
AK1903	57.512531	-152.450838	86.1	Paleogene Pluton	46.5 ± 2.4	9.4 ± 0.9
AK1905	57.610437	-153.984116	0.0	Kodiak Fm.	53.9 ± 3.3	-
AK1907	58.425533	-152.517855	0.0	Uyak Complex	52.2 ± 2.0	19.7 ± 4.4
AK1910	58.353702	-152.222284	0.0	Kodiak Fm.	46.0 ± 0.7	-

* Italic font indicates the youngest grain ages and the 2σ analytical uncertainties of the samples show highly dispersed grain ages. Other ages are mean grain ages and their standard errors.



Citation on deposit: Fan, S., Morell, K. D., Fisher, D. M., Raimbourg, H., Famin, V., & Rajič, K. (2025). Active, long-lived upper-plate splay faulting revealed by thermochronology in the Alaska subduction zone. *Earth and Planetary Science Letters*, 650, Article 119140. <https://doi.org/10.1016/j.epsl.2024.119140>

For final citation and metadata, visit Durham Research Online URL:

<https://durham-repository.worktribe.com/output/3347980>

Copyright statement: This accepted manuscript is licensed under the Creative Commons Attribution 4.0 licence.

<https://creativecommons.org/licenses/by/4.0/>